Electronic Supplementary Information

CVD-grown TiO_2 particles as light scattering structures in dye-sensitized solar cells

Meysam Pazoki,[a,b] Nima Taghavinia,[a,*] Yaser Abdi,[c] Fariba Tajabadi,[a] Gerrit Boschloo [a,*] and Anders Hagfeldt[b]

S1. Factors responsible for differences in growth in Chemical Vapour Deposition

The following factors can explain the difference between the zones quantitatively

a. The difference in the temperature of furnace zones (as mentioned above and measured with an external thermometer) and the gradient exist in the temperature profile of CVD tube reactors because of fluid dynamics of reactant gases can be an important factor affecting the growth. It has been shown that at the higher temperatures, TiO_2 nanoparticles were synthesized from the chemical vapor before the deposition on the surface (J Nanopart Res (2011) 13:5257–5264). It leads to achieve nanostructures with different morphology and crystal structure.
b. Concentration and partial pressure of reactants also have a profile among the tube length. Consequently, crystal formation can be affected by these parameters. Highly porous surface with fine structures (such as shown in Figure 1.b and 1.c) can be obtained by a low deposition rates. Also residence time and collision rate of reactant monomers will have promising changes during the tube length. Different deposition rates between zone A and Zone C can be explained by different reactant concentration.
c. Thickness of boundary layer of inlet gases (Δ) is proportional to the square root of distance (x) from the inlet of gases in the CVD tube, see Eq. 1.[32] μ, ρ and u are viscosity, mass density and flow velocity in the tube, respectively. The thickness of the boundary layer and hence the growth kinetics will change as function of distance in the tube.

$$\Delta = \sqrt{\frac{x\mu}{\rho u}} \quad (1)$$

S2: Tuning the size of CVD-grown particles:

Increase of the temperature leads to a decrease in particle size and Increasing flow rates leads to an increase in particle size. These trends are in agreement with previous work and can be explained by reaction, coagulation- sintering mechanism. Figure S1 shows SEM micrographs of TiO_2 particle films deposited under different conditions and clearly illustrates that by tuning the conditions of growth, spheres with different diameters can be obtained.

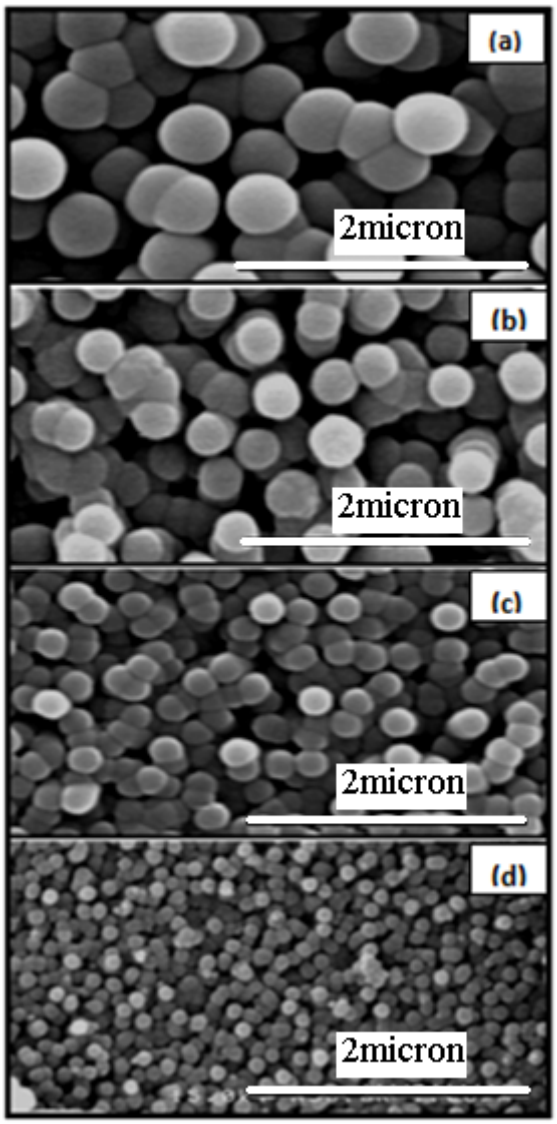

FIG. S1. CVD TiO_2 particle-films grown under different conditions with yielding sphere diameters of (a) 500 nm (b) 300 nm (c) 200 nm and (d) 100 nm. Conditions are: (a) T = 230 ^oC, flow rates of $N_2(TiCl_4)$, O_2 and $Ar(H_2O)$ are 530, 530 and 30 sccm, respectively. (b) T = 265 ^oC, flow rates 530, 530, 30 sccm. (c) T = 245 ^oC, flow rates 390, 390, 30 sccm. (d) T = 245 ^oC, 330, 330, 15 sccm.

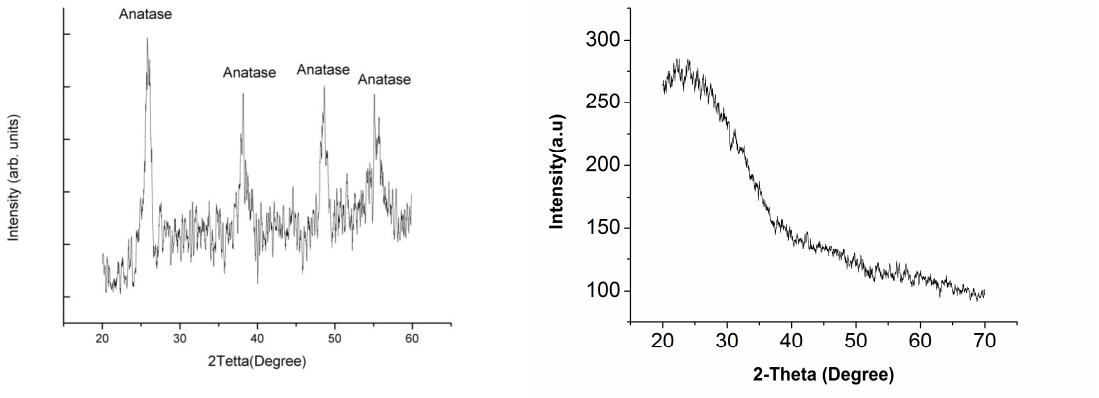

FIG. S2. (a) XRD graph of TiO_2 spheres annealed at 450 °C. (b) XRD graph of as-deposited TiO_2 nanostructures on glass

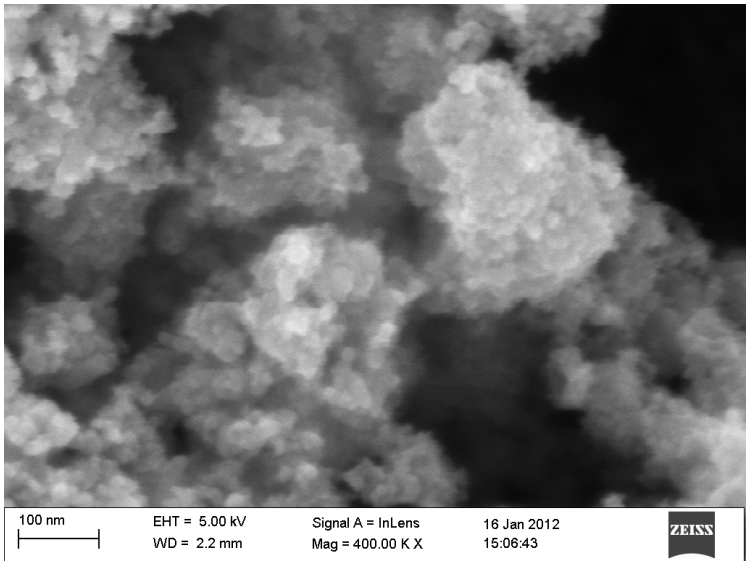

FIG. S3. High resolution SEM of the CVD light-scattering film

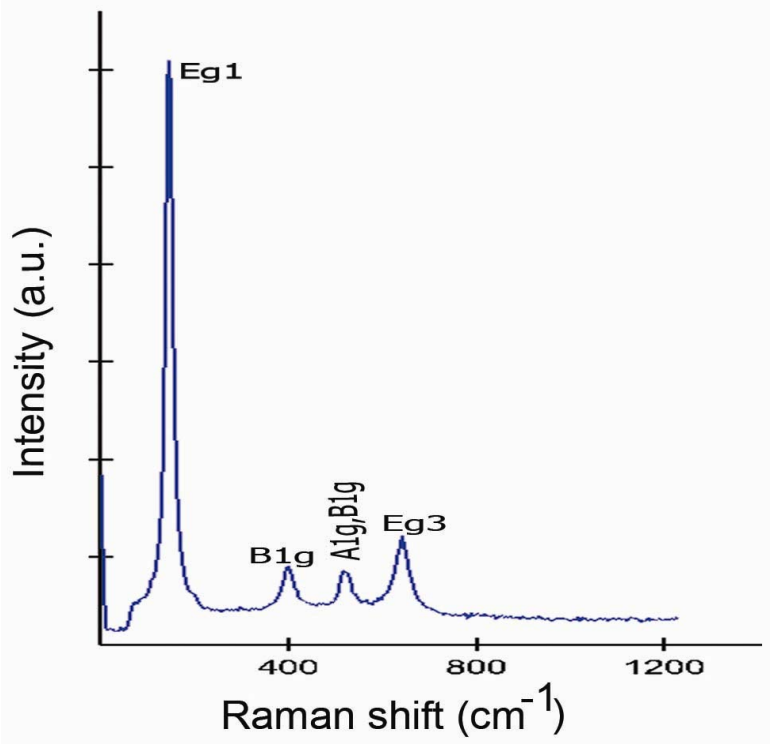

Fig. S4. Raman spectrum of TiO_2 particles on the glass substrate. The spectrum shows TiO_2 anatase peaks at 149, 400, 516 and 637 cm^{-1}.

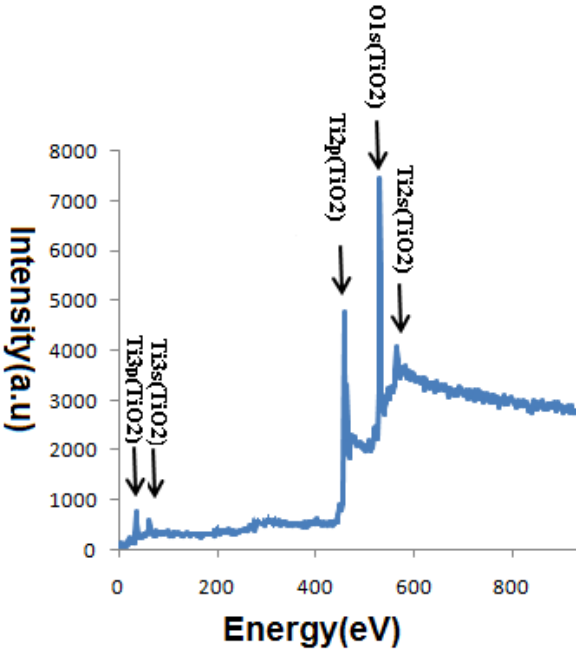

Fig. S5. XPS spectra of CVD paste after annealing

S3. DSC fabrication method using direct growth of CVD scattering particles

FTO (fluorine doped tin oxide) substrate were $TiCl_4$ pretreated in a 40mM $TiCl_4$ solution at 70 ^oC for 30 min. A conventional transparent TiO_2 paste (20 nm particles in ethylcellulose and terpineol) was deposited on FTO by the doctor blade method. Samples were positioned in zone A in the CVD reactor, where spherical TiO_2 particles are deposited on top of the transparent film. The electrodes were heated to 490 ^oC for 30 min, and dye loaded in a 0.3mM ethanolic solution of N719 (cis-di(thiocyanato)-N,N'-bis(2,2'-bipyridyl-4-carboxylic acid-4'-tetrabutylammonium carboxylate) ruthenium(II)) dye for 16h. The counter electrode was made by thermal decomposition of drop cast H2PtCl6 on FTO substrate and heating at 500 ^oC for 30 min. The working-counter electrodes were sealed using 30 μm thick Surlyn sealants. The electrolyte consisted of 0.1 M I_2, 0.1 M LiI, 0.6 M tetrabutylammonium iodide and 0.5 M 4-tert butylpyridine in acetonitrile. J-V curves of the solar cells were recorded under AM1.5 solar simulator (Luzchem Solar).

TiO_2 spheres were deposited on top of a transparent mesoporous TiO_2 film (~ 5 μm thickness) on FTO in the CVD reactor. This resulted in a highly light-scattering layer, suitable as a reflector a in a dye-sensitized solar cells. Fig. S6a shows a SEM micrograph of the deposited scattering spheres. DSC devices were prepared and tested. Fig. S6b shows the current-voltage characteristics of DSCs with and without a scattering sphere layer. A significant increase in the photocurrent density of the cells is observed, clearly demonstrating the good properties of light scattering sphere layer enhancing the light harvesting efficiency. Table S1 shows the photovoltaic parameters of the cells. The presence of scattering layer results in about 60% improvement in the cell efficiency, while the open circuit potential is slightly decreased due to larger interface area of TiO_2 electrode with electrolyte.

TABLE S1. The Photovoltaic properties of DSCs with/without scattering layer

	V_{oc}(V)	J_{sc}(mA/cm^2)	FF(%)	η (%)
With scattering layer	**0.78**	**10.0**	**58**	**4.53**
Without scattering layer	**0.80**	**5.9**	**62**	**2.83**

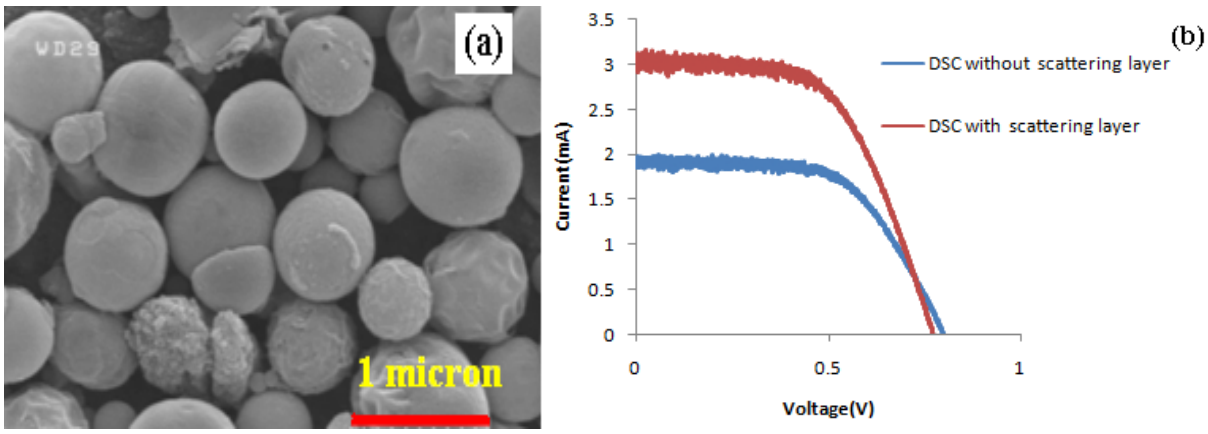

FIG. S6. (a) SEM graph of scattering spheres coated on top of a transparent mesoporous TiO_2 film (b) current voltage characteristics of DSCs with/without scattering layer

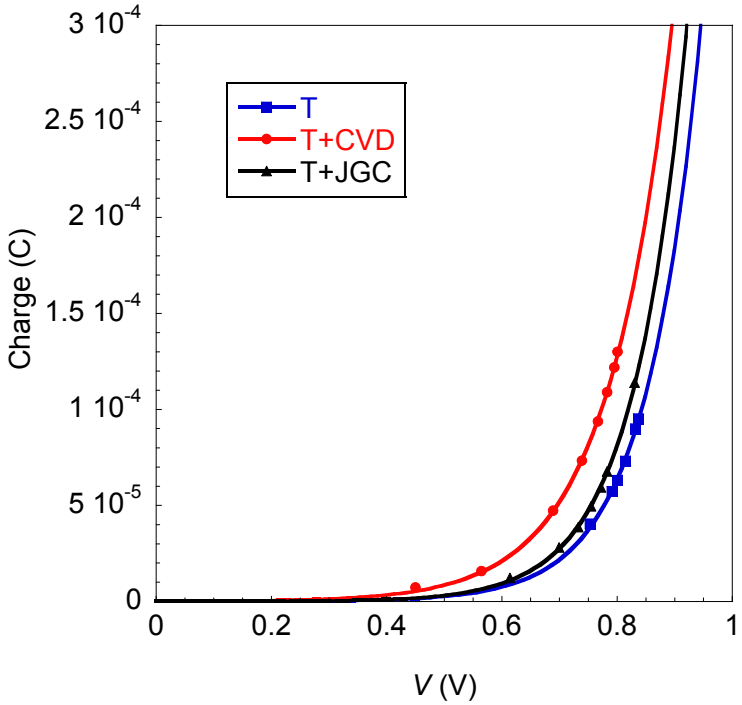

Fig. S7. Fits of trap state distribution according to Eq. 1.

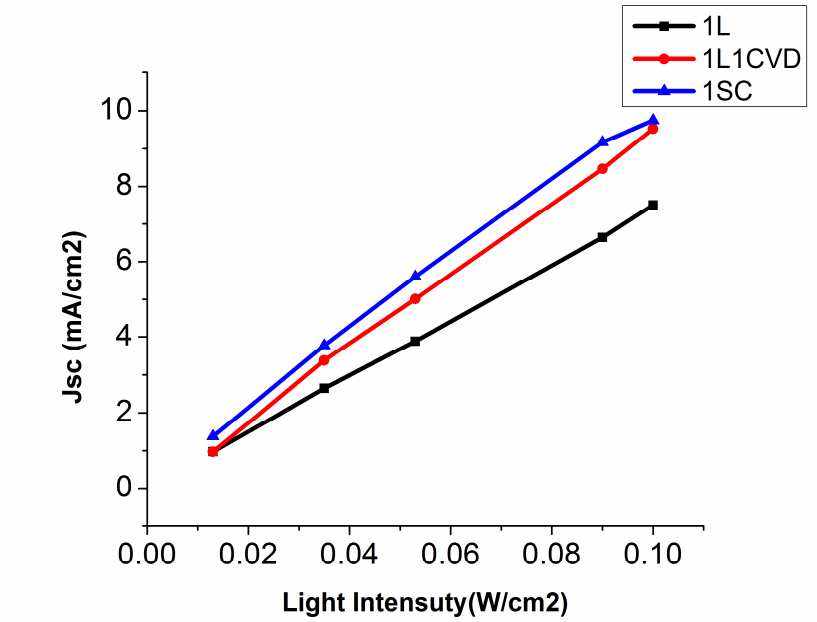

Fig. S8 Short circuit current density of solar cells versus light intensity